ELECTRON BEAM DIAGNOSTICS FOR SHORT PULSE FEL SCHEMES AT CLARA

S. Spampinati#, University of Liverpool and The Cockcroft Institute, Cheshire, U.K
D. Newton, University of Liverpool, Liverpool, U.K

Abstract

CLARA (Compact Linear Accelerator for Research and Applications) [1] is a proposed 250 MeV, 100-400 nm FEL test facility at Daresbury Laboratory. The purpose of CLARA is to test and validate new FEL schemes in areas such as ultra-short pulse generation, temporal coherence and pulse-tailoring. Some of the schemes that can be tested at CLARA depend on a manipulation of the electron beam properties with characteristic scales shorter than the electron beam and require a 30 - 50 µm modulation of the beam energy acquired via the interaction with an infrared laser beam in a short undulator. In this article we describe the electron beam diagnostics required to carry on these experiments.

INTRODUCTION

Some of the most advanced schemes proposed to improve FEL performance depend on a manipulation of the electron beam properties with characteristic scales of several coherence lengths and shorter than the electron beam [2, 3, 4]. We are interested to test, among other schemes, mode locking FEL and femto-slicing for the production of trains of short pulses [5, 6, and 7]. The implementation of these schemes at CLARA requires a 30 - 50 µm modulation of the beam energy acquired via the interaction with an infrared laser beam in a short undulator (modulator). The performance of these FEL schemes depend on this energy modulation. So monitoring the longitudinal phase space of the electron beam is important to perform and to realize these experiments. A deflecting cavity [8] installed in the last part of the FEL line will allow the longitudinal beam distribution to be observed on a screen placed after the dipole leading to the beam dump. Figure 1a shows the FEL line of CLARA, composed of a modulator, a dispersive section, seven radiators and an afterburner section. The afterburner is composed by a series of short undulators and delay chicanes. A possible layout of the diagnostic system placed at the end of the CLARA undulator from the afterburner is shown in Fig. 1b.

In this design, the electron beam is deflected vertically by the deflecting cavity. This deflection maps the electron beam longitudinal coordinate to the vertical coordinate on an intercepting screen after the spectrometer dipole magnet; the dipole converts the particle's energy to the screen horizontal coordinate. Consequently, the electron beam longitudinal phase space is imaged on the screen, and the energy modulation taking place in the modulator can be studied and optimized. Another interesting application of this diagnostic beam line could be the study of the FEL process taking place in the different operation modes of CLARA.

#simone.spampinati@cockcroft.ac.uk

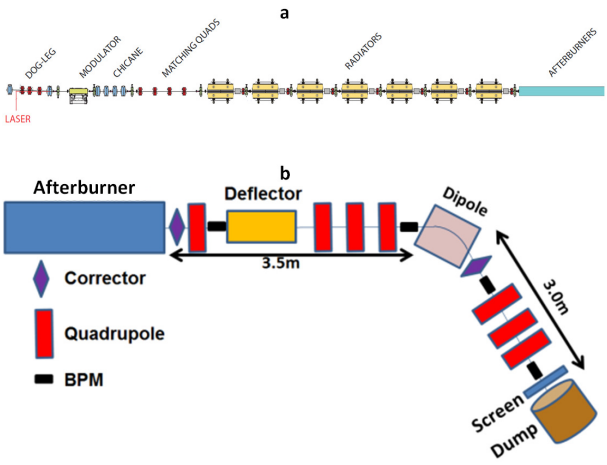

Figure 1: Top: FEl line of CLARA. Bottom: Layout of the phase space diagnostics composed by of a transverse deflector and an energy spectrometer.

OPTICS OPTIMIZATION AND RESOLUTIONS

The vertical beam size at the screen, after deflection, is [9]:

$$\sigma_y = \sqrt{\sigma_{y,0}^{\ 2} + (S\sigma_Z)^2} \qquad (1)$$

where $\sigma_{y,0}$ is the vertical beam size at the screen location without deflection, σ_z is the longitudinal beam size and S is the calibration factor representing the strength of the beam deflection [9]:

$$S = \frac{e_0 V k}{pc}\sqrt{\beta_{yS}\beta_{yD}}\left|\sin\Delta\Psi\right| \qquad (2)$$

here $k = \frac{2\pi}{\lambda}$ with λ = 10.01cm for an S-band cavity (frequency of 2.998 GHz). V_0 is the deflecting voltage, $\beta_{y,D}$ and $\beta_{y,S}$ are vertical betatron functions at the deflector and the screen, respectively. ΔΨ is the vertical

betatron phase advance between the deflector and the screen. The size of the image of the beam detected on the screen will be increased by the system resolution (screen and CCD pixel size) and:

$$\sigma_y = \sqrt{\sigma_{y,0}{}^2 + \sigma_{screen}{}^2 + (S\sigma_Z)^2} \qquad (3)$$

where σ_{Screen} is the screen and CCD resolution.

The longitudinal resolution of the screen image, $\sigma_{L,r}$, can be defined as the ratio of the non-deflected beam size on the screen to the calibration factor S [10]:

$$\sigma_{L,r} = \frac{pc}{e_0 Vk|\sin\Delta\Psi|}\sqrt{\frac{\varepsilon_n}{\gamma\beta_{yD}} + \frac{(\sigma_{screen})^2}{\beta_{yS}\beta_{yD}}} \qquad (4)$$

The third term in equation 3 is equal to the quadratic sum of first two terms when $\sigma_z = \sigma_{L,r}$. The energy resolution of the spectrometer can be written as [10]:

$$\sigma_E = \sqrt{\frac{E^2}{\eta^2}\frac{\varepsilon_n\beta_x}{\gamma} + \frac{E^2}{\eta^2}(\sigma_{screen})^2 + (e_o Vk)^2\frac{\beta_y\varepsilon_n}{\gamma}} \qquad (5)$$

Here η is the horizontal dispersion at the screen. The first two terms represent the resolution of an energy spectrometer line, the third term is the energy spread induced by the deflector [11]. Equations 4 and 5 guide the optimization of the optics functions in the diagnostic beam line. The optimum phase advance between the deflector and the screen is $\Delta\psi = 90^\circ$. Large values of V and $\beta_{y,D}$ lead to a good longitudinal resolution but increase the energy resolution of the system via the induced energy spread. A large value of $\beta_{y,S}$ improves the total longitudinal resolution for a poor resolution screen but has to be narrowed to limit the total beam dimension on the screen given by equation 1. A small value of $\beta_{x,S}$ and a large value of η are required to have a good energy resolution.

STUDY OF BEAM ENERGY MODULATION

Figure 2 shows a possible optical solution, used to study the energy modulation (with a spatial period in the range 30-50 μm), from the entrance of the modulator to the screen. The radiators are at maximum gap and the intra-undulator quadrupoles are used along with the seven quadrupoles shown in Fig. 1 to give the required resolution. The optics shown are for beam energy of 150 MeV. The vertical betatron functions at the deflector and at the screen are 25 m and 0.95 m respectively. The calibration factor S, for a deflecting peak voltage of 5 MV and a RF frequency of 2.998 GHz, is ~10.2. The vertical rms beam size on the screen is 2.7 mm. The horizontal betatron function and dispersion at the screen are 1 m and 0.6 m. A longitudinal resolution of 4.7 μm and an energy resolution of 75 Kev are therefore achieved. A screen resolution of 20 μm is assumed.

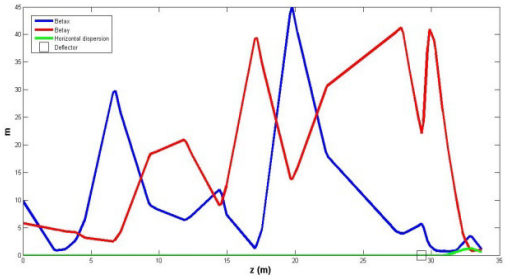

Figure 2: Possible optics from the exit of the modulator to the screen.

Similar optics and performances can be reached for beam energy of 250 MeV with a deflecting voltage of 7.5 MeV.

The reconstruction of the phase space requires short portions of the bunch to be resolved at the screen. An estimate of the length of these portions of the bunch, that can be resolved, can be obtained by using the following simple approach [1, 12]: A portion of the longitudinal density distribution is modelled by two identical Gaussians with different centres in the bunch at a distance Δz. The sigma of the two Gaussians is σ_{screen} /s. This longitudinal test density distribution is reproduced in Fig. 3a. At the screen the separation between the two Gaussians is S·Δz while the sigma is $\sqrt{(\sigma_{y,0})^2 + (\sigma_{screen})^2}$. The vertical profile of the image on the screen is reproduced in Fig. 3b.

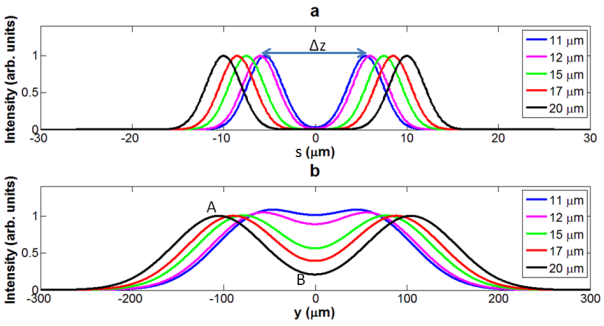

Figure 3: Top: Test longitudinal distributions represented by two Gaussians with a sigma of σ_{Screen} /S separated by a distance Δz. Bottom: Vertical profile on the screen for the distribution depicted above. A and B indicate respectively the values of the intensity of the peaks and of the central local minimum for any profile.

Figure 4a shows the screen image obtained by simulation tracking the test distribution, it representing two Gaussians separated by 16 µm, from the deflector entrance to the screen. The vertical profile of the image on the screen is reproduced in Fig. 4b.

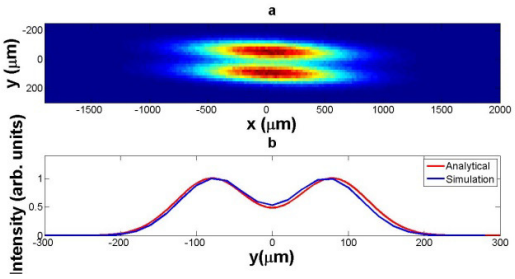

Figure 4: Top: screen image obtained by simulation tracking the test distribution, that it representing two Gaussians separated by 16 µm, from the deflector entrance. Bottom: Vertical profile on the screen.

We can define an intensity contrast IC as (A-B)/A (see Fig. 3b). This parameter quantify the visibility of the separation between the two Gaussians on the screen and for a given measurement system (optics, deflector, screen and CCD) it depends on the separation between the two Gaussians. IC equal to one means perfect visibility while IC equal to 0 means that the image of the two Gaussians are superimposed. The value of IC, for a given measurement system (optics, deflector, screen and CCD) depends on the separation between the two Gaussians. Thus a minimum distance between the two peaks is determined by fixing an intensity contrast. The intensity contrast as function of the distance between the two peaks is plotted in Fig. 5 for the system described above. A value of IC close to 0.5 is obtained when the two Gaussians in the beam distribution are at a distance of 15 µm. This is a first estimate of the minimum slice length detectable [1].

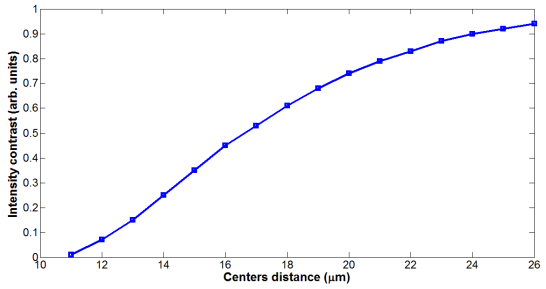

Figure 5: IC vs centers distance.

Simulations including the beam energy modulation in the modulator, the vertical deflection in the RF deflector and the beam transport up to the screen have been performed with the code ELEGANT [13] to test the performance of the diagnostic system introduced above. The parameters used in the simulations are listed in Table 1 and are taken from the CLARA CDR [1]. One-dimensional longitudinal space charge (LSC) and coherent synchrotron radiation (CSR) impedances are included in the simulations.

Table 1: Simulation Parameters

Parameter	Value	Unit
Macro-particles	$2 \cdot 10^6$	
Beam energy	150	MeV
Energy spread	50 (RMS)	Kev
Emittance	0.6 (RMS)	mm-mrad
Laser wavelength	40	µm
Laser pulse duration	500 (FWM)	fs
Laser pulse energy	10	µJ
Laser waist	2.5	mm
Deflecting frequency	2.998	GHz
Deflecting voltage	5	MV
Screen resolution	20 (RMS)	µm

Results of simulation are shown in Fig. 6. Fig. 6a shows the phase space after the interaction in the modulator (see Fig. 1) with the 40 µm laser. Fig. 6b shows the beam density distribution projected on the x-y plane at the end of the diagnostic beam line and it representing the screen image. The energy modulation is well evident as predicted above.

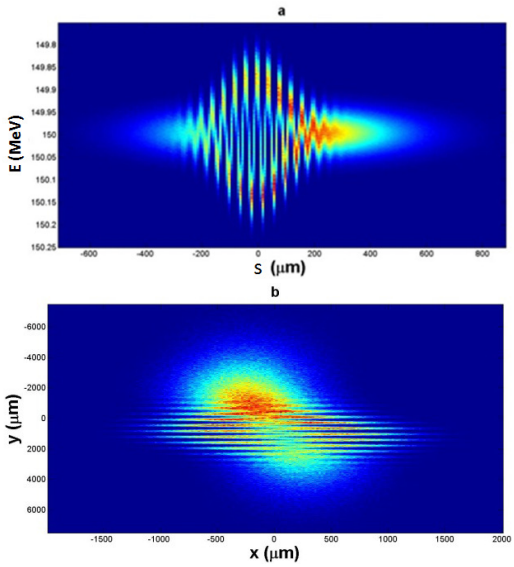

Figure 6: Top: Beam phase space after the interaction in the modulator (see Fig. 1) with the laser. Bottom: beam density distribution projected on the x-y plane at the end of the diagnostic beam line.

We can now compere the beam energy modulation after the laser-electron interaction with the measurements on the screen. We can derive the beam energy modulation on the screen image by using the theoretical value of the calibration factor S (eq. 2) and of the horizontal dispersion at the screen location. Linear correlated energy spread induced by the deflector, LSC and CSR can be removed. The result is shown in Fig. 7 where the mean slice energy is plotted versus the slice longitudinal coordinate in the bunch. The red curve is the beam energy modulation derived by screen analysis (Fig. 6b) and the blue is the energy modulation present on the beam after the laser-electron interaction in the modulator (Fig. 6a). The agreement between the two curves is good.

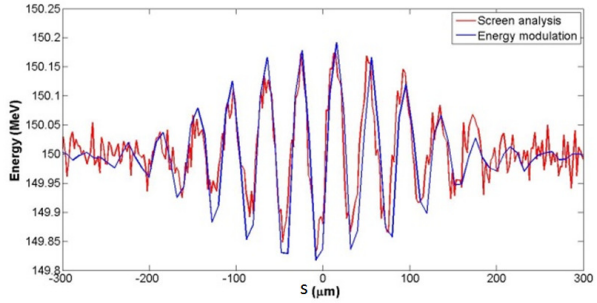

Figure 7: Beam energy modulation derived by the measurement analysis (red) compared with the one gained in the modulator (blue).

ENERGY MODULATION START UP

The interaction between the laser and the electron in the modulator requires a temporal and a spatial alignment of the two beams. The diagnostics so far described can be used to find the effects of the laser-electron interaction during these procedures.

A spatial pre-alignment can be done by aligning the long wavelength laser (30-50 μm) beam with the 800 nm laser that will be used in the seeding experiments [1] and aligning this laser beam with the electron beam on two OTR [14] or CROMOX (Al2O3:Cr) [15] screens placed at both ends of the modulator. Alternatively two OTR screens can be used to image directly the long wavelength laser beam and the electrons using a Pyro electric Array Camera instead of a CCD to look at the two screens. We have performed the same simulation of the energy modulation adding a transverse off-set and a tilt to the laser respect to electron beam trajectory in the modulator in order to estimate the required alignment tolerances. Figure 8 shows the phase space imaged on the screen when there are off-sets of 2 mm between the laser and the electron beam in both planes and the laser trajectory is tilted by 0.002 rad respect to the electron beam trajectory tilt. The laser modulation is still well evident. We can quantify these values of off-sets and tilt as the requirements for the initial alignment between the laser and the electron beam. This level of alignment can be reached rather easily with the pre-alignment. The alignment can be improved after having established the interaction using remote movable mirror to maximize the energy modulation on the screen.

In the same way a coarse overlapping (with an accuracy of 200-300 ps) in time between the two beam can be established recording on the same oscilloscope a signal for the electron beam coming from a BPM pickup and a signal for the laser from a photodiode placed on an optical table in the linac tunnel closer possible to the modulator and to each other. The temporal overlapping can be adjusted by scanning a delay line for the laser while observing the spectrometer screen.

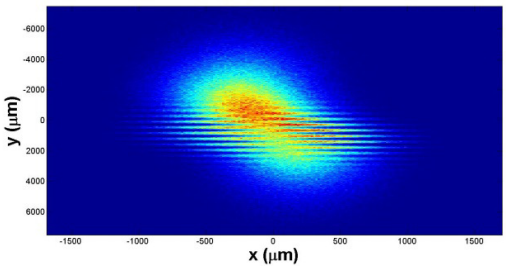

Figure 8: Beam imaged on the spectrometer screen as obtained by a simulation with the code Elegant for the parameter reported in Tb. 1 adding a relative laser-electron beam misalignment of 2 mm in both planes at the entrance of the undulator and a tilt of 2 mrad for the laser trajectory.

STUDY OF THE FEL INTERACTION

Recently a method to study FEL pulse length and fel intensity using a defector and an electron beam spectrometer has been proposed and applied to LCLS experiments [16, 17]. The beam phase space is measured with the FEL on and the FEL off. The application of the energy conservation principle permits to measure the temporal profile of the FEL pulse (E. vs t.) from the changes in the slice mean energy and energy spread induced by the lasing.

The diagnostics described above can be used to study the electron beam phase space with the FEL process on and off to apply this method. In this case the radiators are closed and the intra-radiator qudrupoles are set to ensure beta values required by FEL. We can use the quadrupoles placed after the last radiator to optimize the diagnostics resolutions according to eq. 4 and eq. 5. A quadrpupole in the middle of the afterburner has been considered in this case. A possible solution for the optics between the last radiator and the spectrometer screen is shown in Fig. 9. The vertical betatron functions at the deflector and at the screen are 60 m and 0.95 m respectively. The calibration factor S, for a defecting voltage of 5 MV and a RF frequency of 2.998 GHz, is ~16.2. The horizontal beta and dispersion at the screen are 1m and 0.6m.

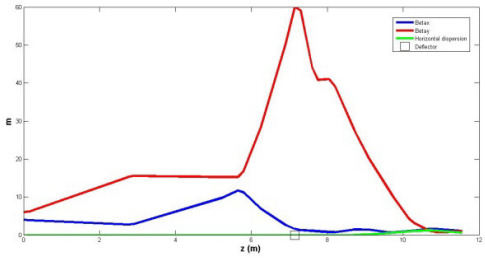

Figure 9: Possible optics from the exit of last radiator to the screen.

For this solution a longitudinal resolution of 3.3 µm and an energy resolution of 105 Kev are predicted by equations 4 and 5. A value of IC close to 0.5 is obtained for two features in the beam distribution separated by a distance of 10 µm as can be seen in Fig. 10.

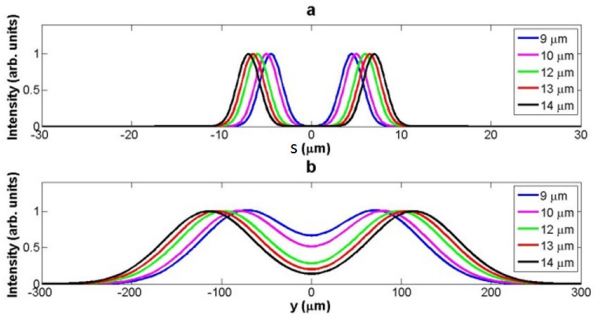

Figure 10: Top: longitudinal test distributions. Bottom: Vertical profiles at screen.

Simulations including the FEL process, using the codes GENESIS [18] and ELEGANT, will be performed.

CONCLUSIONS

We have presented results on the viability of post-FEL diagnostics on CLARA to study the phase space of the beam after the beam energy modulation required by mode locking and sliced FEL schemes. Their expected performance and simulations of their utilization have been presented.

ACKNOWLEDGEMENTS

This work is funded by STFC (Science and Technology Facilities Council, UK). We thank S. Di Mitri, P. Williams and N. Thompson for the careful reading and suggestions.

REFERENCES

[1] J. A. Clarke et al., JINST **9**, 05 (2014).
[2] A.A. Zholents, W.M. Fawley, Phys. Rev. Lett. **92**, 224801, (2004).
[3] E. Kur, D.J. Dunning, B.W.J. McNeil, J. Wurtele, A.A. Zholents, New J. Phys. **13**, 063012 (2011).
[4] D.J. Dunning, B.W.J. McNeil, N.R. Thompson, Phys. Rev. Lett. **110**, 104801 (2013).
[5] E.L. Saldin, E.A. Schneidmiller, M.V. Yurkov, Phys. Rev. ST Accel. Beams **9**, 050702 (2006).
[6] N. R. Thompson, B.W.J. McNeil, Phys. Rev. Lett. **100**, 203901 (2008).
[7] L. Giannessi et al., Phys. Rev. Lett. **106**, 144801 (2011).
[8] G. A. Loew, O.H. Altenmueller, SLAC, PUB-135, Aug. (1965).
[9] Y. Ding et al., "Ultra-short electron bunch and X-ray temporal diagnostics with an x-band transverse deflecting cavity", in Proc. 1st Int. Beam Instrumentation Conf., Tsukuba, Japan Accelerator (2012), TUPA41.
[10] Y. Ding et al., "Commissioning of the X-band Transverse Deflector for Femtosecond Electron / X-Ray Pulse Length Measurements at LCLS", in Proc. 4th Int. Particle Accelerator Conf., Shanghai, (2013), WEOBB201.
[11] M. Cornacchia, P. Emma, Phys. Rev. ST Accel. Beams **5**, 084001 (2002).
[12] P. Craievich et al., "A transverse RF deflecting cavity for FERMI@elettra project", in Proc. 8th European Workshop on Beam Diagnostics and Int. for Particle Accelerator Conf., Venice, (2007), TUPC10.
[13] M. Borland, ANL/APS Report No. LS-287 (2000).
[14] Z. Huang et al., Phys. Rev. ST Accel. Beams **13**, 020703 (2010).
[15] S. Spampinati et al., "Commissioning of the FERMI@ELETTRA Laser Heater", in Proc. 34th International Free-Electron Laser Conference, Nara, (2012), MOPD58.
[16] Y. Ding et al., Phys. Rev. ST Accel. Beams **14**, 120701 (2011).
[17] C. Behrens at al., Nature communications **5**, 3762 (2014).
[18] S. Reiche et al., Nucl. Instrum. Methods Phys. Res., Sect. A 429, 243 (1999).